Microfluid Nanofluid (2015) 18:103–109
DOI 10.1007/s10404-014-1417-8

RESEARCH PAPER

Viscous dissipation effect in nano-confined shear flows: a comparative study between molecular dynamics and multi-scale hybrid simulations

Jie Sun · Wen Wang · Hua Sheng Wang

Received: 14 December 2013 / Accepted: 2 May 2014 / Published online: 16 May 2014

Abstract In this work, a full molecular dynamics simulation (MDS) of nano-confined shear flows has been conducted to examine the effect of viscous dissipation and applicability of multi-scale hybrid simulation. In the cases of high shear rate and strong solid–liquid interaction, the difference is clearly seen between the MDS and hybrid simulation results. The applicability of the hybrid simulation is found highly dependent on the effect of viscous dissipation. The non-monotonic variation of the average temperature found in pressure-driven flows is also found in the present shear-driven flows. By comparatively analyzing the molecular dynamics and hybrid simulation results, it is confirmed that the hybrid simulation is valid and the explicit correlation between the slip and Kapitza lengths is valid in the ranges of shear rate ($\dot{\gamma} = 0.012-0.094\ \tau^{-1}$, τ being the time scale) and solid–liquid interaction factor ($\beta = 0.1$–10). Although the hybrid simulation results deviate from the MDS results due to the effect of viscous dissipation, the explicit correlation between the slip and Kapitza lengths still holds.

1 Introduction

Surface wettability, determined by the surface free energy, has been an important topic recently due to its highly potential application in various fields (Bocquet and Barrat 2007; Rauscher and Dietrich 2008; Roach et al. 2008; Shirtcliffe et al. 2010; Drelich et al. 2011; Yan et al. 2011). For example, hydrophobicity could be used for anti-bacteria, anti-corrosion, self-cleaning, drag reduction (Qu et al. 2004; Truesdell et al. 2006; Roach et al. 2008), while hydrophilicity is applicable to anti-fogging, biofouling, contact lenses, bone-like structures and enhancement of boiling heat transfer (Drelich et al. 2011).

In micro/nano-channel studies, it has been found that surface wettability plays an essential role in drag reduction and heat transfer performance (Xue et al. 2003; Qu et al. 2004; Truesdell et al. 2006; Kim et al. 2008; Cao et al. 2009; Li et al. 2010). The surface wettability microscopically originates from the solid–liquid interaction, therefore, determines the resistance of the momentum and energy transportation across the solid–liquid interface. The velocity slip (u_s) and temperature jump (T_j), defined as the velocity and temperature differences between the wall and liquid adjacent to it, respectively, are the characteristic quantities. For example, a superhydrophobic surface could give a giant velocity slip (Lee et al. 2008), while a superhydrophilic surface (Thompson and Robbins 1990) could lead to a negative velocity slip. In practice, the slip length (L_s) is widely used to quantify the degree of u_s, according to the linear Navier boundary condition, as (Gad-el-Hak 1999):

$$L_s = u_s \Big/ \left.\frac{\partial u}{\partial n}\right|_w \tag{1}$$

Similarly, the Kapitza length (L_K) is widely used to quantify the degree of T_j as (Kim et al. 2008):

$$L_K = T_j \Big/ \left.\frac{\partial T}{\partial n}\right|_w \tag{2}$$

where $(\partial u/\partial n)|_w$ and $(\partial T/\partial n)|_w$ are the velocity and temperature gradients of a liquid at wall surface,

J. Sun (✉)
Institute of Engineering Thermophysics,
Chinese Academy of Sciences, Beijing 100190, China
e-mail: j.sun@qmul.ac.uk

J. Sun · W. Wang · H. S. Wang (✉)
School of Engineering and Materials Science,
Queen Mary, University of London, London E1 4NS, UK
e-mail: h.s.wang@qmul.ac.uk

respectively. Accurate predictions of L_s and L_K are crucial for design of micro/nano-fluidic devices because experiments have proved that the velocity and temperature profiles greatly deviates from the analytical solutions (Swartz and Pohl 1989; Choi et al. 2003; Joseph and Tabeling 2005; Truesdell et al. 2006; Byun et al. 2008). The problem is complicated because it is influenced by many parameters such as the solid–liquid interaction (Thompson and Robbins 1990; Thompson and Troian 1997; Xue et al. 2003; Priezjev 2007; Soong et al. 2007; Kim et al. 2008; Liu and Li 2009; Kim et al. 2010; Liu et al. 2010), commensurability of solid and liquid densities (Thompson and Robbins 1990; Thompson and Troian 1997), solid structure (Soong et al. 2007), surface geometry (Cao et al. 2006), surface temperature (Kim et al. 2008), driving force (Liu and Li 2009; Liu et al. 2010), shear rate (Priezjev 2007; Kim et al. 2010), flow rate (Liu and Li 2009; Liu et al. 2010), viscous dissipation (Kim et al. 2010), temperature gradient (Kim et al. 2008). Among all these factors, the solid–liquid interaction has been widely accepted as the predominant one. On the other hand, although L_s and L_K are qualitatively counterparts, it is not easy to measure both *simultaneously* in nano-confined liquid flows though L_s is measurable by microparticle image velocimetry (micro-PIV) measurement (Joseph and Tabeling 2005; Truesdell et al. 2006; Byun et al. 2008; Lee et al. 2008) and L_K is accessible via time resolved reflectivity or absorption measurement (Gavrila et al. 2009), separately. Therefore, a correlation between L_s and L_K is important. Recently, we have found such explicit correlations between L_s and L_K in Couette-type (shear-driven) flows (Sun et al. 2013a):

$$L_K/\sigma = 2.3, \beta > 2 \tag{3a}$$

$$L_K/\sigma = 2.3 + 0.04(L_s/\sigma)^{2.8}, \beta \leq 2 \tag{3b}$$

where σ is the length characteristic parameter, $\beta = \varepsilon_{sl}/\varepsilon$ is the proportional factor of solid–liquid bonding strength (ε_{sl} and ε being the energy characteristic parameters for solid–liquid and liquid–liquid interactions, respectively).

It has been found that the decoupling emerges and the hybrid simulation becomes invalid when $U > 3.0\ \sigma\tau^{-1}$ in shear flows (Sun et al. 2013a), where U is the driving velocity, and $\tau = \sqrt{m\sigma^2/\varepsilon}$ is the characteristic time (m being the mass of a liquid molecule). As was pointed out, this is solely related to the viscous dissipation. To clarify, in the present work, the nano-confined shear flows are studied using full molecular dynamics simulation (MDS) in order to (1) show the effects of viscous dissipation on the velocity, temperature and density profiles and (2) examine the applicability of the hybrid simulation and validity of the correlation between L_s and L_K.

2 Simulation method

The modified Lennard-Jones (L-J) potential function (1973) is used for liquid–liquid interaction:

$$\varphi(r) = 4\varepsilon\left\{\left[\left(\frac{\sigma}{r}\right)^{12} - \left(\frac{\sigma}{r}\right)^{6}\right] + \left[6\left(\frac{\sigma}{r_c}\right)^{12} - 3\left(\frac{\sigma}{r_c}\right)^{6}\right]\left(\frac{r}{r_c}\right)^{2} - \left[7\left(\frac{\sigma}{r_c}\right)^{12} - 4\left(\frac{\sigma}{r_c}\right)^{6}\right]\right\} \tag{4}$$

where r is the intermolecular separation and $r_c = 2.5\ \sigma$ is the cutoff radius. The solid–liquid interaction is also described by Eq. (4) but with different length and energy characteristic parameters of $\sigma_{sl} = 0.91\ \sigma$ and $\varepsilon_{sl} = \beta\varepsilon$. The value of β varies from 0.1 to 10, corresponding to the surface free energy from low to high. This approach has been widely used in MDS studies due to its simplicity and clear physical meaning (Thompson and Robbins 1990; Thompson and Troian 1997; Xue et al. 2003; Priezjev 2007; Kim et al. 2008; 2010).

Shear-driven flow conducted in a planar nano-channel with two confining surfaces separated by a distance $H = 54.5\sigma$ is considered in the present work (see Fig. 1). The overall system size is $l_x \times l_y \times l_z = 28.5\text{-}\sigma \times 7.0\sigma \times 60.1\sigma$, where l_i, $i = x, y, z$ are the dimensions in x, y and z directions. The channel height is $H = 54.4\sigma$. The two parallel walls are kept at a constant temperature T_w with the upper wall moving at a constant velocity U. The periodic boundary conditions are used in horizontal directions. Two atomically smooth walls are arranged at the upper and lower sides in parallel. Each wall is represented by 3 layers of solid atoms in face-centered cubic (111) pattern normal to z-axis with the lattice constant of $\sigma_s = 0.814\ \sigma$ (therefore $\rho_s = 2.62\ \sigma^{-3}$), where σ_s and ρ_s are the characteristic length and number density of solid, respectively. Neighboring atoms are connected by Hookean springs with the constant $k = 3{,}249.1\varepsilon\sigma^{-2}$ (Yi et al. 2002). Two extra layers of atoms are set below/above the lower/upper walls (Maruyama 2000; Sun et al. 2009). The outmost layers are stationary as a frame while the second outmost layers are governed by the Langevin thermostat.

$$\frac{d\mathbf{p}_i(t)}{dt} = -\alpha\mathbf{p}_i(t) + \mathbf{f}_i(t) + \mathbf{F}_i(t) \tag{5}$$

where t is time; $\mathbf{p}_i(t)$ is the momentum vector of ith atom; $\mathbf{f}_i(t)$ is the interaction force vector between ith atom and its neighbors; $\mathbf{F}_i(t)$ is the exciting force vector, of which the components are randomly sampled from the Gaussian distribution with mean $\mu_G = 0$ and standard deviation $\sigma_G = \sqrt{2\alpha k_B T_w/\delta t}$ ($\alpha = 168.3\tau^{-1}$ being the damping constant, $k_B = 1.38 \times 10^{-23}$ J K^{-1} being the Boltzmann constant, $T_w = 1.1\ \varepsilon k_B^{-1}$ being the preset wall temperature

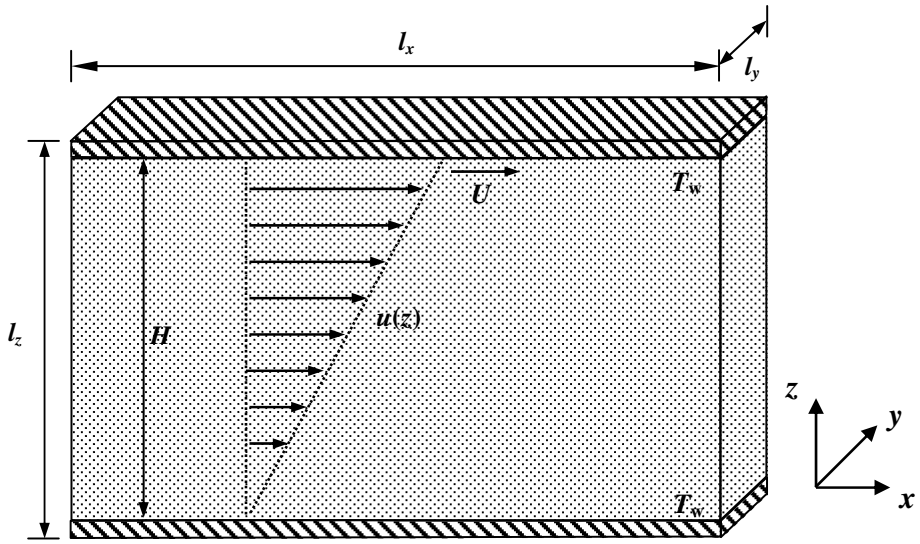

Fig. 1 Schematic of computational model

and $\delta t = 0.005\ \tau$ being the time step). The overall solid atom number is 3,500.

The system is initialized by 8,928 liquid molecules uniformly arranged between the walls with the number density $\rho = 0.81\ \sigma^{-3}$. A period of 200 τ is used for thermal equilibrium at $T = 1.1\ \varepsilon k_B^{-1}$. The following 6,000 τ is the production period, during which the upper wall velocity is kept constant at $U = 1.0$–$5.0\ \sigma\tau^{-1}$. The sampling is carried out every time step, and the averaging is over the final 2,000 τ. The leapfrog scheme is used for integrating the equations of motion, and the cell subdivision technique is employed to improve the computational efficiency (Allen and Tildesley 1987; Rapaport 2004).

Note that the system size is the same, but the boundary conditions at the upper wall are different between the hybrid simulations (Sun et al. 2013b) and the present MDSs. In the hybrid simulation, the liquid near the upper wall is solved by the finite volume method with no slippage at the interface while in the present MDSs, slippage exists at both upper and lower interfaces.

3 Results and discussion

The u-velocity, temperature and density profiles with $\beta = 0.1$–10 and $U = 1.0$–$5.0\ \sigma\tau^{-1}$ are shown in Fig. 2. For a given U, all the profiles are significantly influenced by β. u_s varies from positive to negative with increasing β because liquid molecules could move freely under weak solid–liquid interaction, i.e., small β, while strong interaction, i.e., large β, tends to trap the liquid molecules around. The shear rate $\dot{\gamma}$ is found to increase correspondingly. A non-monotonic variation of temperature profile is seen. When $\beta \leq 4$, the temperature profile is found to drop as a whole and T_j correspondingly decreases. Afterward, T_j exists within the liquid rather than at the solid–liquid interface and remains almost constant but the maximum value of the temperature taking at the middle increases when $\beta > 4$. The density profiles clearly show fading oscillation in liquid away from the wall surface due to the, experimentally proved, layering structure near the solid–liquid interface (Magnussen et al. 1995; Regan et al. 1995; Huisman et al. 1997). At least five peaks, the range of which is about 4.9σ, can be clearly seen, indicating that the five layers of liquid molecules are more influenced by the solid–liquid interaction than by the liquid–liquid interaction. Based on the competition between the boundary and bulk factors (Sun et al. 2013b), the liquid adjacent to the solid is referred to as the boundary region, where the liquid molecules would experience the combined effect of β and $\dot{\gamma}$, while the rest of the liquid is referred to as the bulk region, where the boundary-related effect (β) is absent. The amplitude of the oscillation increases with increasing β because stronger solid–liquid interaction tends to keep the liquid molecules stacked more densely. Due to the strong solid–liquid interaction ($\beta > 2$), the first one or two layers of liquid molecules within the boundary region are completely dominated by β and behave like extensional solid with the u-velocity, temperature and density all very close to those of the solid.

On the other hand, the effect of viscous dissipation becomes more intensive with increasing $\dot{\gamma}$; the maximum value of the temperature generally rises from $1.14 - 1.18\ \varepsilon k_B^{-1}$ ($U = 1.0\ \sigma\tau^{-1}$) to $1.99 - 2.40\ \varepsilon k_B^{-1}$ ($U = 5.0\ \sigma\tau^{-1}$). The large rise in temperature profile due to large $\dot{\gamma}$, in turn, changes $\dot{\gamma}$ from uniform to non-uniform, especially for large β cases (see Fig. 2c). The density profile varies diversely due to viscous dissipation; the

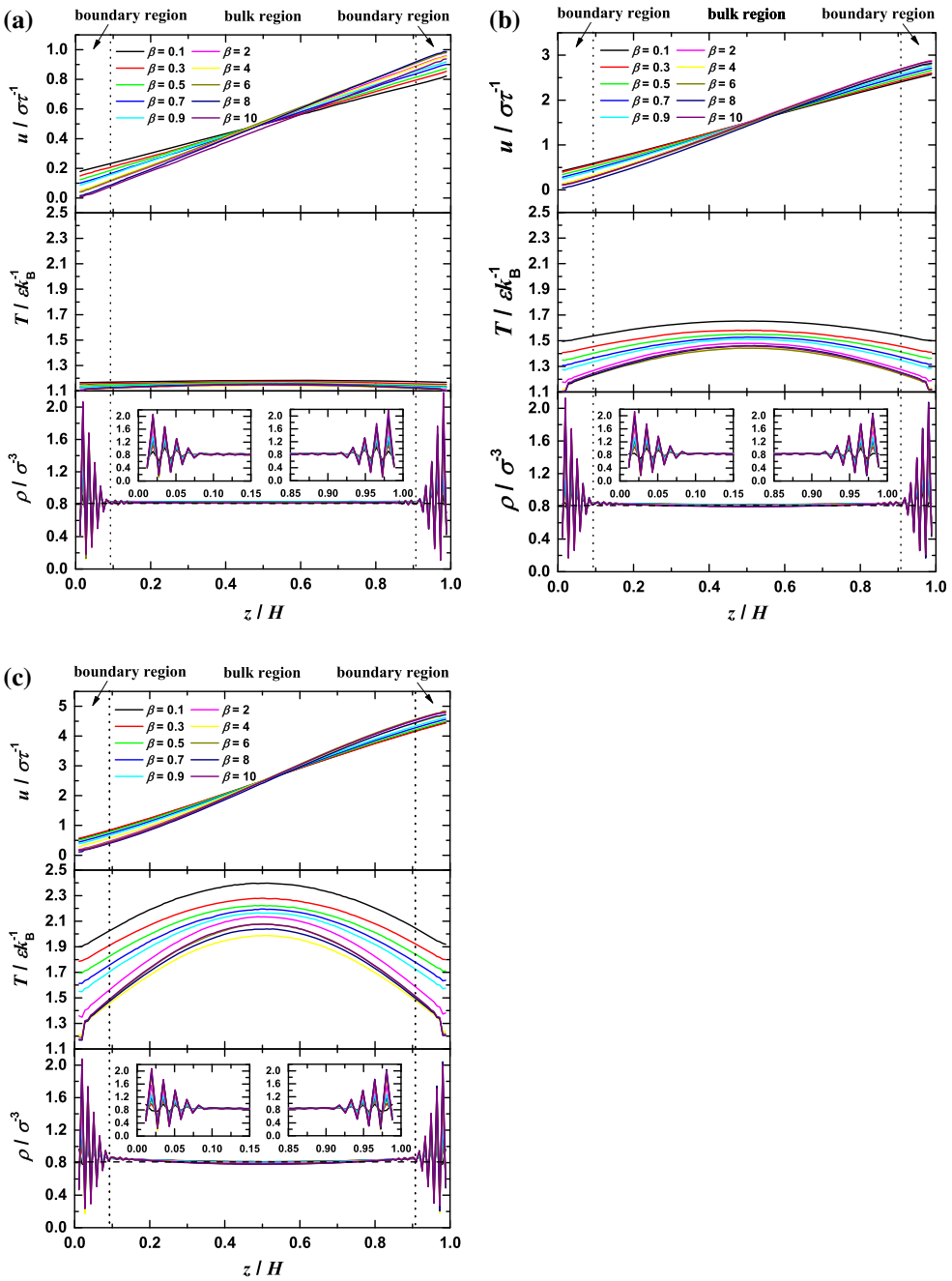

Fig. 2 (Color online) u-velocity, temperature and density profiles at **a** $U = 1.0\ \sigma\tau^{-1}$ **b** $U = 3.0\ \sigma\tau^{-1}$ and **c** $U = 5.0\ \sigma\tau^{-1}$. The *dash lines* show constant density at $\rho = 0.81\ \sigma^{-3}$

density in the boundary region does not show appreciable change, while that in the bulk region bends lower at the middle and rises at the ends, showing weak thermal expansibility and compressibility of the liquid.

The aforementioned non-monotonic variation of the temperature profile is a result of typically competitive phenomenon, as was discussed in the Poiseuille flows (Sun et al. 2013b). To clearly illustrate this, we take the average temperature T_{ave} instead of the whole temperature profile for analysis. Figure 3a shows the energy balance between the viscous dissipation rate per unit volume Φ ($=\int_0^H 2\mu\dot{\gamma}\mathrm{d}z$, μ being the dynamic viscosity) in the liquid and the heat flux q ($=T_j/R_K$, R_K being the interfacial thermal resistance) at the solid–liquid interface. For a given U, on the one hand, increasing β means decreasing R_K (Xue et al. 2003), which reduces T_j, therefore T_{ave} tends to decrease; on the other hand, increasing β results in decrease in u_s (see Fig. 2) and consequently increase in $\dot{\gamma}$, which increases Φ, therefore T_{ave} tends to increase. For clarity, the analysis is simply expressed as for a given U, $\beta\uparrow \rightarrow R_K\downarrow \rightarrow T_j\downarrow \rightarrow T_{ave}\downarrow$, meanwhile, $\beta\uparrow \rightarrow u_s\downarrow \rightarrow \dot{\gamma}\uparrow \rightarrow \Phi\uparrow \rightarrow T_{ave}\uparrow$. The opposite influences of β on T_{ave} form a competitive

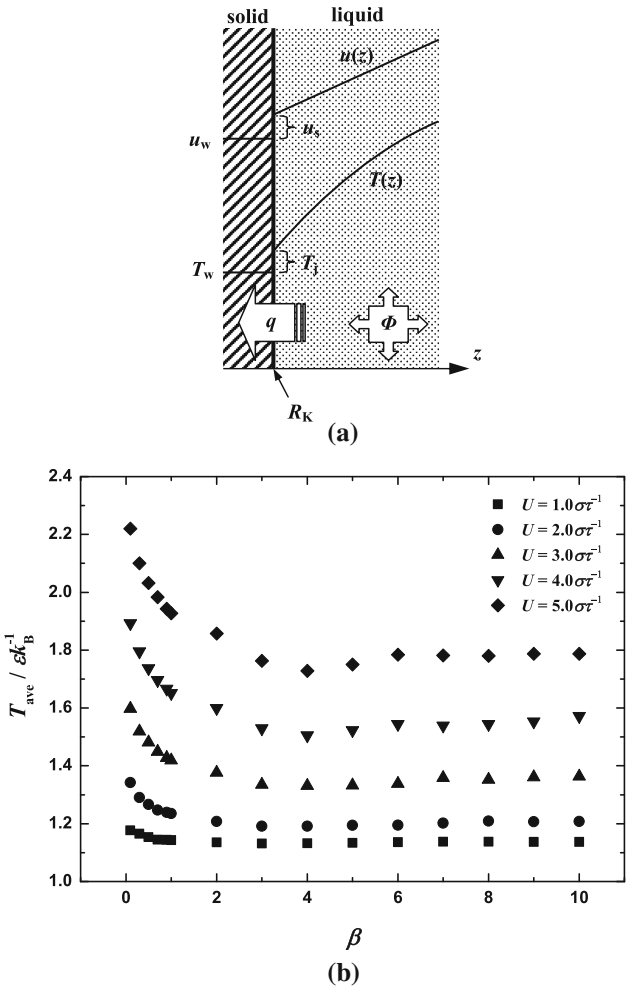

Fig. 3 **a** Schematic of heat transfer and **b** variation of average temperature (T_{ave}) against solid–fluid bonding factor (β)

condition and an extremum are predictable. Figure 3b shows the variations of T_{ave} with β for different U. The minimum values of T_{ave} are clearly seen at $\beta \approx 4$. It is also found that for a given β, T_{ave} monotonically increases with U. The reason can be expressed as for a given β, $U\uparrow \rightarrow \dot{\gamma}\uparrow \rightarrow \Phi\uparrow \rightarrow T_{ave}\uparrow$.

In Fig. 4a, L_s and L_K are seen to be nonlinearly decreasing functions of β with a threshold of $\beta = 2$. They quickly drop when $\beta \leq 2$ and become scattered when $\beta > 2$, especially for L_s, because the solid–liquid interaction is strong that the one or two layers of liquid molecules adjacent to the wall behave as extensional solid and consequently the velocity slip and temperature jump are found within the liquid rather than at the solid–liquid interface (see Fig. 2). This diverse variation agrees well with our hybrid simulation results (Sun et al. 2013a) and Thompson and Robbins' work (Thompson and Robbins 1990). In Fig. 4b, L_s and L_K are seen as decreasing functions of $\dot{\gamma}$. If viscous dissipation is negligible, $u(z)$ varies as a linear function of $\dot{\gamma}$, i.e., $u(z) = \dot{\gamma}z + u_s$.

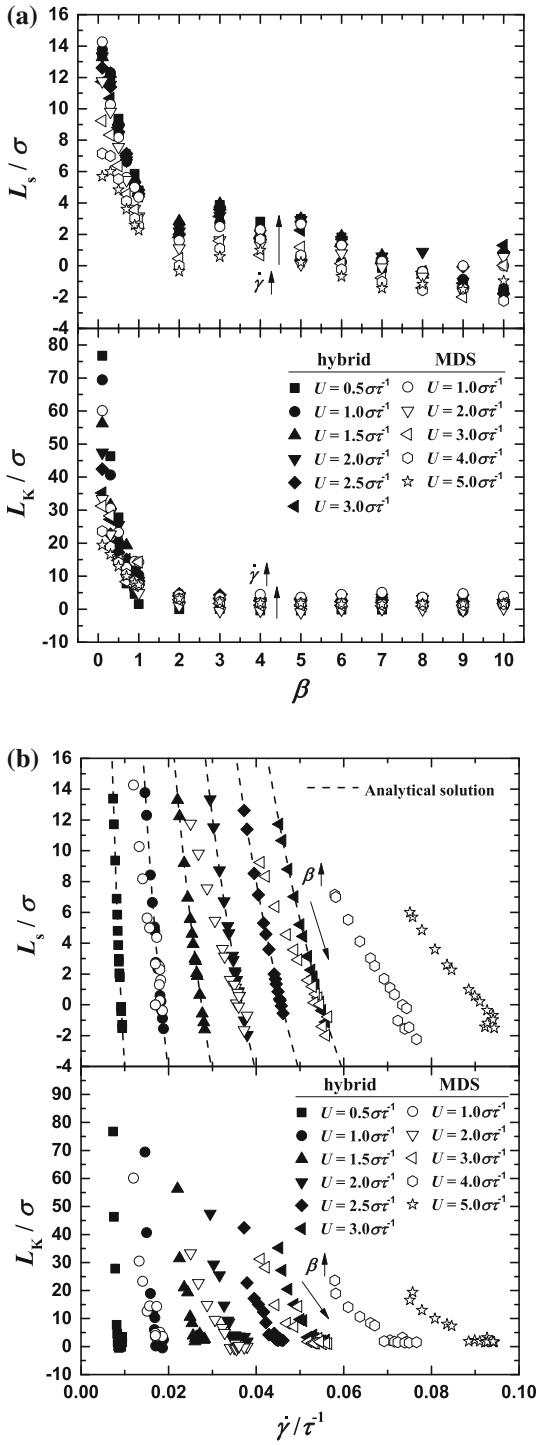

Fig. 4 Variations of slip length (L_s) and Kapitza length (L_K) against **a** solid–fluid bonding factor (β) and **b** shear rate ($\dot{\gamma}$). The hybrid simulation results are taken from (Sun et al. 2013a)

Considering $u(H) = U$ and $L_s = u_s/\dot{\gamma}$, we have $L_s = U/\dot{\gamma} - H$, which is also plotted in Fig. 4b. The hybrid simulation results are found to agree well with the analytical solutions because the shear rate is low and the dissipation

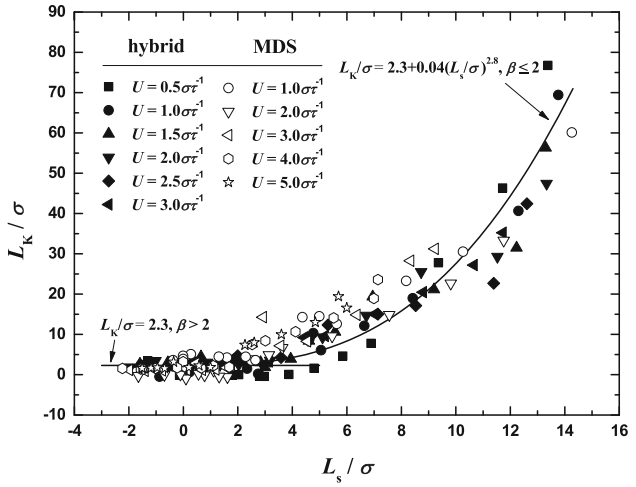

Fig. 5 Variation of Kapitza length (L_K) against slip length (L_s). The hybrid simulation results are taken from (Sun et al. 2013a)

effect is weak. In fact, it had been found that the decoupling emerges and the hybrid simulation becomes invalid when $U > 3.0\ \sigma\tau^{-1}$. When the viscous dissipation is weak (i.e., low shear rate cases), the MDS results agree with the analytical solutions, whereas when the viscous dissipation is strong (i.e., high shear rate cases), the MDS results apparently deviate from the analytical solutions. Similar trend is also seen in the variation of L_K against $\dot{\gamma}$. Besides, it is found that for a given β, L_K is essentially a decreasing function of $\dot{\gamma}$ when $\beta \le 2$ and L_K becomes much less sensitive to β when $\beta > 2$.

The variation of L_K against L_s is summarized covering all the cases in Fig. 5. Good agreement is seen between the present MDS and hybrid simulation results (Sun et al. 2013a) even though the velocity range in the present MDS is larger. The general correlation between L_K and L_s is presented based on the data fitting of all the simulation results. Note that the effects of $\dot{\gamma}$ and β are implicitly included. Since the scenarios and mechanisms are different for small β ($\beta \le 2$) and large β ($\beta > 2$) cases, L_K is found basically constant when $\beta > 2$, while it grows as a power function of L_s when $\beta \le 2$. Therefore, the correlation has different forms, as shown in Eq. (3a, 3b). This different form again emphasizes that the solid–liquid interaction plays a dominant role in the boundary region. It is noteworthy that Eq. (3a, 3b) is refitted using only the present MDS results, and it does not show appreciable change (see Fig. 5). Therefore, it is confirmed that Eq. (3a, 3b) is valid within $U = 1.0$–$5.0\ \sigma\tau^{-1}$ ($\dot{\gamma} = 0.012 - 0.094\ \tau^{-1}$) and $\beta = 0.1$–10. In fact, the dissipation effect has already been taken into account. This strongly suggests that L_K and L_s may have inherent correlation and no matter how L_s is generated, e.g., identical L_s by different combinations of $\dot{\gamma}$ and β, L_K varies correspondingly following Eq. (3a, 3b) regardless of $\dot{\gamma}$. Moreover, it has been confirmed the applicability of the hybrid simulation (Sun et al. 2013b).

Note that the computational cost for the hybrid simulation is remarkably cheaper as it is generally proportional to the particle numbers involved and could be largely saved further considering the application of symmetric boundary condition and flexible region decomposition (Sun et al. 2012). Besides, it is shown recently that the computational efficiency could be further increased by improvement of time-step coupling (Lockerby et al. 2013).

4 Concluding remarks

In this work, a full MDS of nano-confined shear flows has been performed. The molecular dynamics results are compared with the hybrid simulation ones. It is demonstrated that the applicability of the hybrid simulation is highly dependent on the effect of viscous dissipation. The previously revealed non-monotonic variation of the average temperature in pressure-driven flows by the hybrid simulation is also found in shear-driven flows by MDS. It is confirmed that Eq. (3a, 3b) is valid within $U = 1.0$–$5.0\ \sigma\tau^{-1}$ ($\dot{\gamma} = 0.012 - 0.094\ \tau^{-1}$) and $\beta = 0.1$–10. The fact that although the dissipation effect causes deviation in hybrid simulation results from MDS results, the correlation between L_s and L_K still holds, indicating an inherent correlative dependence.

Acknowledgments Financial supports from the Beijing Natural Science Foundation (3142021) and the Engineering and Physical Sciences Research Council (EPSRC) of the UK (EP/L001233/1) are acknowledged.

References

Allen MP, Tildesley DJ (1987) Computer simulation of liquids. Clarendon Press, Oxford

Bocquet L, Barrat JL (2007) Flow boundary conditions from nano- to micro-scales. Soft Matter 3(6):685–693

Byun D, Kim J, Ko HS, Park HC (2008) Direct measurement of slip flows in superhydrophobic microchannels with transverse grooves. Phys Fluids 20(11):113601

Cao BY, Chen M, Guo ZY (2006) Liquid flow in surface-nanostructured channels studied by molecular dynamics simulation. Phys Rev E 74:066311

Cao BY, Sun J, Chen M, Guo ZY (2009) Molecular momentum transport at fluid-solid interfaces in MEMS/NEMS: a review. Int J Mol Sci 10(11):4638–4706

Choi CH, Westin KJA, Breuer KS (2003) Apparent slip flows in hydrophilic and hydrophobic microchannels. Phys Fluids 15(10):2897–2902

Drelich J, Chibowski E, Meng DD, Terpilowski K (2011) Hydrophilic and superhydrophilic surfaces and materials. Soft Matter 7(21):9804–9828

Gad-el-Hak M (1999) The fluid mechanics of microdevices: the freeman scholar lecture. J Fluids Eng T ASME 121(5):5–33

Gavrila G, Godehusen K, Weniger C, Nibbering ETJ, Elsaesser T, Eberhardt W, Wernet P (2009) Time-resolved X-ray absorption spectroscopy of infrared-laser-induced temperature jumps in liquid water. Appl Phys A 96(1):11–18

Huisman WJ, Peters JF, Zwanenburg MJ, de Vries SA, Derry TE, Abernathy D, van der Veen JF (1997) Layering of a liquid metal in contact with a hard wall. Nature 390(6658):379–381

Joseph P, Tabeling P (2005) Direct measurement of the apparent slip length. Phys Rev E 71(3):035303

Kim BH, Beskok A, Cagin T (2008) Molecular dynamics simulations of thermal resistance at the liquid-solid interface. J Chem Phys 129:174701

Kim BH, Beskok A, Cagin T (2010) Viscous heating in nanoscale shear driven liquid flows. Microfluid Nanofluid 9(1):31–40

Lee C, Choi C-H, Kim C-JC (2008) Structured surfaces for a giant liquid slip. Phys Rev Lett 101(6):064501

Li Y, Xu J, Li D (2010) Molecular dynamics simulation of nanoscale liquid flows. Microfluid Nanofluid 9(6):1011–1031

Liu C, Li Z (2009) Flow regimes and parameter dependence in nanochannel flows. Phys Rev E 80(3):036302

Liu C, Fan HB, Zhang K, Yuen MMF, Li ZG (2010) Flow dependence of interfacial thermal resistance in nanochannels. J Chem Phys 132(9):094703

Lockerby DA, Duque-Daza CA, Borg MK, Reese JM (2013) Time-step coupling for hybrid simulations of multiscale flows. J Comput Phys 237:344–365

Magnussen OM, Ocko BM, Regan MJ, Penanen K, Pershan PS, Deutsch M (1995) X-ray reflectivity measurements of surface layering in liquid mercury. Phys Rev Lett 74(22):4444–4447

Maruyama S (2000) Molecular dynamics method for microscale heat transfer. In: Minkowycz WJ, Sparrow EM (eds) Advances in numerical heat transfer, vol 2. Tayler & Francis, New York, pp 189–226

Priezjev NV (2007) Rate-dependent slip boundary conditions for simple fluids. Phys Rev E 75(5):051605

Qu J, Perot B, Rothstein JP (2004) Laminar drag reduction in microchannels using ultrahydrophobic surfaces. Phys Fluids 16(12):4635–4643

Rapaport DC (2004) The art of molecular dynamics simulation. Cambridge University Press, Cambridge

Rauscher M, Dietrich S (2008) Wetting phenomena in nanofluidics. Ann Rev Mater Res 38:143–172

Regan MJ, Kawamoto EH, Lee S, Pershan PS, Maskil N, Deutsch M, Magnussen OM, Ocko BM, Berman LE (1995) Surface layering in liquid gallium: an x-ray reflectivity study. Phys Rev Lett 75(13):2498–2501

Roach P, Shirtcliffe NJ, Newton MI (2008) Progress in superhydrophobic surface development. Soft Matter 4(2):224–240

Shirtcliffe NJ, McHale G, Atherton S, Newton MI (2010) An introduction to superhydrophobicity. Adv Colloid Interface Sci 161(1–2):124–138

Soong CY, Yen TH, Tzeng PY (2007) Molecular dynamics simulation of nanochannel flows with effects of wall lattice-fluid interactions. Phys Rev E 76(3):036303

Stoddard SD, Ford J (1973) Numerical experiment on the stochastic behavior of a Lennard-Jones gas system. Phys Rev A 8(3):1504–1512

Sun J, He YL, Tao WQ (2009) Molecular dynamics-continuum hybrid simulation for condensation of gas flow in a microchannel. Microfluid Nanofluid 7(3):407–422

Sun J, He YL, Tao WQ, Yin X, Wang HS (2012) Roughness effect on flow and thermal boundaries in microchannel/nanochannel flow using molecular dynamics-continuum hybrid simulation. Int J Numer Methods Eng 89(1):2–19

Sun J, Wang W, Wang HS (2013a) Dependence between velocity slip and temperature jump in shear flows. J Chem Phys 138(23):234703

Sun J, Wang W, Wang HS (2013b) Dependence of nanoconfined liquid behavior on boundary and bulk factors. Phys Rev E 87(2):023020

Swartz ET, Pohl RO (1989) Thermal boundary resistance. Rev Mod Phys 61(3):605–668

Thompson PA, Robbins MO (1990) Shear flow near solids: expitaxial order and flow boundary conditions. Phys Rev A 41(12):6830–6837

Thompson PA, Troian SM (1997) A general boundary condition for liquid flow at solid surfaces. Nature (London) 389(6649):360–362

Truesdell R, Mammoli A, Vorobieff P, van Swol F, Brinker CJ (2006) Drag reduction on a patterned superhydrophobic surface. Phys Rev Lett 97(4):044504

Xue L, Keblinski P, Phillpot SR, Choi SUS, Eastman JA (2003) Two regimes of thermal resistance at a liquid-solid interface. J Chem Phys 118(1):337–339

Yan YY, Gao N, Barthlott W (2011) Mimicking natural superhydrophobic surfaces and grasping the wetting process: a review on recent progress in preparing superhydrophobic surfaces. Adv Colloid Interface Sci 169(2):80–105

Yi P, Poulikakos D, Walther J, Yadigaroglu G (2002) Molecular dynamics simulation of vaporization of an ultra-thin liquid argon layer on a surface. Int J Heat Mass Transfer 45(10):2087–2100